NF-κB–induced R-loop accumulation and DNA damage select for nucleotide excision repair deficiencies in adult T cell leukemia

Yunlong He[a,1], Nagesh Pasupala[a,1], Huijun Zhi[a,1], Batsuhk Dorjbal[b], Imran Hussain[a], Hsiu-Ming Shih[c,d], Sharmistha Bhattacharyya[e], Roopa Biswas[e], Milos Miljkovic[f], Oliver John Semmes[g,h], Thomas A. Waldmann[f], Andrew L. Snow[b], and Chou-Zen Giam[a,2]

[a]Department of Microbiology and Immunology, Uniformed Services University of the Health Sciences, Bethesda, MD 20814; [b]Department of Pharmacology and Molecular Therapeutics, Uniformed Services University of the Health Sciences, Bethesda, MD 20814; [c]Institute of Biomedical Sciences, Academia Sinica, Taipei 11529, Taiwan; [d]Institute of Molecular and Genomic Medicine, National Health Research Institutes, Miaoli County 350, Taiwan; [e]Department of Anatomy, Physiology, and Genetics, Uniformed Services University of the Health Sciences, Bethesda, MD 20814; [f]Center for Cancer Research, National Cancer Institute, NIH, Bethesda, MD 20892; [g]Department of Microbiology and Molecular Cell Biology, Eastern Virginia Medical School, Norfolk, VA 23501; and [h]The Leroy T. Canoles Jr. Cancer Research Center, Eastern Virginia Medical School, Norfolk, VA 23501

Edited by Robert Gallo, Institute of Human Virology and Departments of Medicine and Microbiology and Immunology, University of Maryland School of Medicine, Baltimore, MD, and approved January 7, 2021 (received for review March 25, 2020)

Constitutive NF-κB activation (NF-κB^{CA}) confers survival and proliferation advantages to cancer cells and frequently occurs in T/B cell malignancies including adult T cell leukemia (ATL) caused by human T-cell leukemia virus type 1 (HTLV-1). Counterintuitively, NF-κB^{CA} by the HTLV-1 transactivator/oncoprotein Tax induces a senescence response, and HTLV-1 infections in culture mostly result in senescence or cell-cycle arrest due to NF-κB^{CA}. How NF-κB^{CA} induces senescence, and how ATL cells maintain NF-κB^{CA} and avert senescence, remain unclear. Here we report that NF-κB^{CA} by Tax increases R-loop accumulation and DNA double-strand breaks, leading to senescence. R-loop reduction via RNase H1 overexpression, and short hairpin RNA silencing of two transcription-coupled nucleotide excision repair (TC-NER) endonucleases that are critical for R-loop excision—*Xeroderma pigmentosum* F (XPF) and XPG—attenuate Tax senescence, enabling HTLV-1–infected cells to proliferate. Our data indicate that ATL cells are often deficient in XPF, XPG, or both and are hypersensitive to ultraviolet irradiation. This TC-NER deficiency is found in all ATL types. Finally, ATL cells accumulate R-loops in abundance. Thus, TC-NER deficits are positively selected during HTLV-1 infection because they facilitate the outgrowth of infected cells initially and aid the proliferation of ATL cells with NF-κB^{CA} later. We suggest that TC-NER deficits and excess R-loop accumulation represent specific vulnerabilities that may be targeted for ATL treatment.

NF-κB activation | adult T cell leukemia | R-loop | transcription-coupled nucleotide excision repair | DNA damage

Human T cell leukemia virus type 1 (HTLV-1) is the etiological agent of adult T cell leukemia/lymphoma (ATL). The HTLV-1 viral transactivator/oncoprotein Tax is a potent inducer of IKK/NF-κB (1–4). While constitutive NF-κB activation (NF-κB^{CA}) is a common feature of ATL and confers proliferation and survival advantages to leukemia cells (5–9), we have found that NF-κB^{CA} by Tax induces a rapid senescence response (Tax-IRS) mediated by the cyclin-dependent kinase inhibitors p21$^{Cip1/Waf1}$ (p21) and p27^{Kip1} (p27) during a single cell-cycle passage. Most naive cells newly infected by HTLV-1 also undergo cell-cycle arrest or senescence (10–12). In contrast, ATL and HTLV-1–transformed T cells are resistant to Tax-IRS (13), suggesting that they have acquired genetic/epigenetic changes that overcome senescence and facilitate adaptation to NF-κB^{CA}. Intriguingly, Tax senescence is driven by the transcriptional activity of NF-κB (14). How messenger RNA (mRNA) transcription directed by hyperactive NF-κB leads to senescence and how ATL cells maintain NF-κB^{CA} without becoming senescent remain unclear.

An R-loop is a three-stranded nucleic acid structure consisting of an RNA–DNA hybrid and a displaced single-stranded DNA loop. R-loop formation mediates immunoglobulin isotype switching, CRISPR-mediated DNA excision, transcription-coupled nucleotide excision repair (TC-NER), and chromatin structure and transcription (15, 16). Of special relevance here, transcriptional derepression and RNA splicing/elongation/processing/export deficiencies are known to cause R-loop accumulation, DNA damage and genomic instability (GI) (17). Recent data have further indicated that R-loop excision by the TC-NER endonucleases, Xeroderma pigmentosum F (XPF) and XPG, is responsible for inducing DNA double-strand breaks (DSBs) and GI (15, 18).

Here we demonstrate that HTLV-1 Tax promotes R-loop accumulation, DNA damage, as well as senescence in an NF-κB–dependent manner. Reducing R-loop formation and processing by RNase H1 overexpression and short hairpin RNA (shRNA) silencing of the TC-NER coupling factors XPF, XPG, and Cockayne

Significance

Cellular NF-κB activity is stringently regulated. Constitutive NF-κB activation (NF-κB^{CA}), however, frequently occurs in T/B cell malignancies including adult T cell leukemia (ATL) caused by human T cell leukemia virus type 1 (HTLV-1). We demonstrate that NF-κB^{CA} via the HTLV-1 trans-activator/oncoprotein Tax causes R-loop accumulation, DNA double-strand breaks, and senescence and that R-loop processing by the transcription-coupled nucleotide excision repair (TC-NER) pathway contributes to senescence induction. We show that TC-NER deficits occur in ATL. They enable senescence escape and outgrowth of HTLV-1–infected and ATL cells with NF-κB^{CA}, but render ATL cells hypersensitive to ultraviolet light. With NF-κB^{CA}, ATL cells continue to accumulate abundant R-loops. TC-NER deficiency and excess R-loop accumulation represent vulnerabilities of ATL that can be exploited therapeutically.

Author contributions: Y.H., N.P., H.Z., B.D., A.L.S., and C.-Z.G. designed research; Y.H., N.P., H.Z., B.D., and I.H. performed research; H.-M.S., M.M., T.A.W., and A.L.S. contributed new reagents/analytic tools; Y.H., N.P., H.Z., I.H., S.B., R.B., O.J.S., A.L.S., and C.-Z.G. analyzed data; and C.-Z.G. wrote the paper.

The authors declare no competing interest.

This article is a PNAS Direct Submission.

[1]Y.H., N.P., and H.Z. contributed equally to this work.

[2]To whom correspondence may be addressed. Email: chou-zen.giam@usuhs.edu.

This article contains supporting information online at https://www.pnas.org/lookup/suppl/doi:10.1073/pnas.2005568118/-/DCSupplemental.

Published March 1, 2021.

syndrome group B (CSB) attenuates Tax and NF-κB–induced senescence, allowing cells newly infected by HTLV-1 to proliferate. Interestingly, immunoblotting of ATL cell lines and in silico analyses of ATL patient mRNA microarray data indicate that ATL cells are often deficient in XPG, XPF, and CSB. This renders them highly sensitive to ultraviolet light (UV)-induced cytotoxicity. Finally, many ATL cells continue to accumulate R-loops in abundance, raising the possibility that a restoration of TC-NER function may increase DNA damage in ATL to drive cell-cycle arrest/senescence/apoptosis. We propose that NF-κB hyperactivation by Tax causes excess R-loop accumulation, leading to TC-NER–mediated R-loop processing, DSBs, and senescence. A loss of TC-NER factors, including XPF, XPG, and CSB, reduces R-loop processing, and DNA damage thereby attenuates Tax-IRS to favor proliferative expansion of HTLV-1–infected and ATL cells with NF-κB^{CA}. These results reveal TC-NER deficits and excess R-loop accumulation as specific vulnerabilities of ATL that may be therapeutically exploited.

Results

Tax Induces R-Loop Accumulation, DSBs, and Senescence in an NF-κB–Dependent Manner. Senescence is a cellular mechanism for tumor suppression. Central to senescence induction is DNA damage and the engagement of the DNA damage response (DDR) pathway and tumor suppressors (19–22). Given the importance of DNA damage in senescence induction, we examined whether IKK/NF-κB hyperactivation by Tax results in DNA damage and DDR. To this end, HeLa-G, a Tax reporter cell line containing a GFP reporter, 18 × 21-GFP, under the regulation of 18 copies of the Tax-responsive viral 21-bp-repeat enhancer element, and a HeLa-G–derived cell line, HeLa-G/Δ*N*-IκBα, in which NF-κB is shut off by the constitutive expression of a degradation-resistant form of IκBα, Δ*N*-IκBα, were transduced with Ad-Tax or a control Ad-GFP vector. Twelve hours later, cell lysates were harvested and immunoblotted to detect Tax, IκBα (whose degradation underlies NF-κB activation), p21 and p27 (as markers for Tax-IRS), and γH2AX (as a marker of DSBs) (Fig. 1*A*). Indeed, Tax potently activated NF-κB and elicited a robust DDR with increased γH2AX in HeLa-G (Fig. 1*A*, lane 4), but not in HeLa-G/Δ*N*-IκBα cells where NF-κB is inhibited by Δ*N*-IκBα (23) (Fig. 1*A*, lane 2). As previously shown, p21 and p27 levels rose sharply as a function of NF-κB hyperactivation by Tax, but not when NF-κB was blocked by Δ*N*-IκBα (compare Fig. 1*A*, lanes 2 and 4) (23). As expected, Ad-GFP had no effects (lanes 1 and 3). These data agree with earlier studies showing that Tax causes DSBs and micronuclei formation (24–26) and link the clastogenic effect of Tax to NF-κB hyperactivation.

In an effort to elucidate how NF-κB hyperactivation by Tax drives DNA damage and senescence, we were intrigued by studies in yeast and human cells that demonstrate a critical role of excess R-loop formation in inducing DSBs and genomic instability (15–17, 27–29). Of particular relevance here, R-loops can accumulate cotranscriptionally as a result of RNA polymerase II stalling upon excessive transcriptional activation/de-repression (17). Since the transcriptional activity of NF-κB is causally linked to Tax-induced DNA damage (Fig. 1*A*) and senescence (14), we asked whether excess R-loops accumulated during Tax-mediated NF-κB hyperactivation. To address this question, nucleic acids were extracted from Ad-Tax– or Ad-GFP–transduced HeLa-G and HeLa-G/Δ*N*-IκBα cells and deposited onto nylon membranes using a slot-blot apparatus. The samples were probed with a monoclonal antibody, S9.6, that specifically binds RNA–DNA hybrids (Fig. 1*B*, R-DH). Equal loading of nucleic acids (NA) for each sample was verified by methylene blue staining (Fig. 1*B*, NA). As shown in Fig. 1*B* (R-DH, lane 4), a significant increase in R-loops was observed in HeLa-G, but not in HeLa-G/Δ*N*-IκBα cells transduced by Ad-Tax (lane 2). Ad-GFP control had little effect on either cell line as expected. The

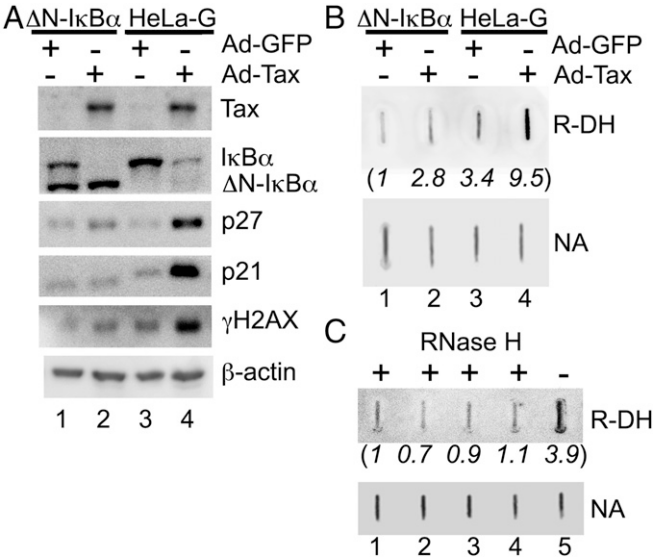

Fig. 1. NF-κB hyperactivation by Tax induces R-loop accumulation and DNA damage. (*A*) HeLa-G and HeLa-G/Δ*N*-IκBα cells were transduced by Ad-Tax or the control Ad-GFP vector (moi: ~5) for 12 h and then immunoblotted with the indicated antibodies. In the presence of Tax, IκBα, but not Δ*N*-IκBα, is constitutively phosphorylated and degraded, becoming barely detectable (lanes 2 and 4). (*B*) Chromosomal nucleic acids were extracted from the transduced cells and slot-blotted (1 μg) with the S9.6 antibody to detect RNA–DNA hybrids (denoted as R-DH) as a marker of R-loop formation. The amount of nucleic acid (marked as NA) loaded in each slot was estimated by methylene blue staining. (*C*) Nucleic acid samples (1 μg each, lanes 1 to 4 as in *B*, were treated with RNase H (NEB M0297, 5 units, 37 °C, 2 h) and slot-blotted with the S9.6 antibody. The untreated sample from Ad-Tax–transduced HeLa-G was included as a positive control (lane 5). The intensity of each band in the blots was quantified using the ImageJ software, normalized first against that of the corresponding NA band, and then the normalized value of lane 1 in each blot, and is shown in parentheses under each lane.

RNA–DNA hybrid signal detected by the S9.6 antibody disappeared upon treatment with RNase H1, consistent with the accumulation of R-loops upon NF-κB hyperactivation by Tax (Fig. 1*C*, lane 5 vs. lane 4). In aggregate, these results support the notion that hyperactivated NF-κB promotes accumulation of R-loops, whose subsequent processing by the TC-NER pathway likely contributes to the induction of DSBs and senescence.

RNase H1 Overexpression Attenuates Tax/NF-κB–Induced Senescence. Overexpression of RNase H1 is known to reduce R-loop accumulation, DSBs, and genome instability (17, 29). To assess the role of R-loop–associated DSBs in Tax-IRS, we generated HeLa-G/RNase H1, a HeLa-G–derived line stably expressing HA-tagged human RNase H1 (Fig. 2*A*, *Upper Left*). The effect of RNase H1 on Tax-IRS was then determined by transducing sparsely plated HeLa-G and HeLa-G/RNase H1 cells with Ad-Tax. Tax expression in reporter cells activates 18 × 21-EGFP (23, 30) to produce strong GFP signals, allowing the fate of single Tax^{+} cells to be monitored microscopically. We have previously shown that Tax-expressing HeLa-G cells progress through the S/G2/M phases of an aberrant cell cycle and become arrested in senescence mostly as single and occasionally as double GFP+ cells (10, 23, 31). As shown in Fig. 2*B* (compare day 1 and day 3 panels), most Ad-Tax–transduced HeLa-G controls never progressed beyond a single-cell division cycle. In contrast, HeLa-G/RNase H1 underwent approximately two to three rounds of cell division with some transduced cells appearing as clusters of four or more GFP+ cells 3 d after Ad-Tax transduction (Fig. 2B, second column

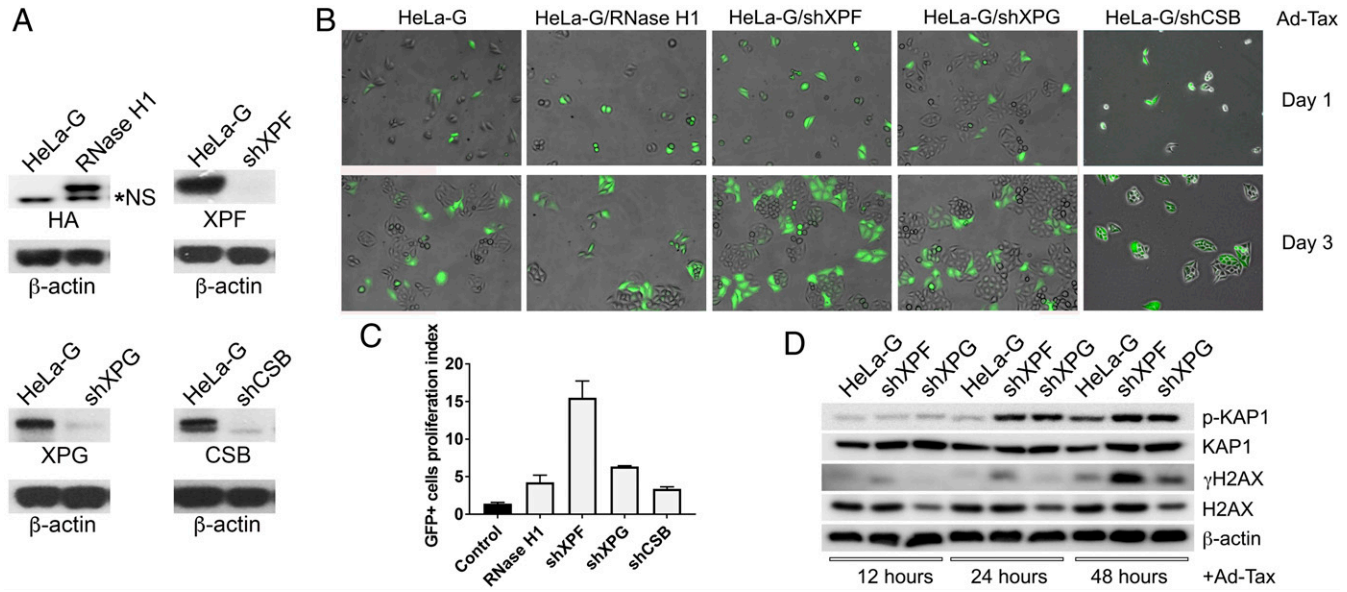

Fig. 2. RNase H1 overexpression and XPF/XPG/CSB knockdown attenuate Tax-IRS. (*A*) Immunoblots of HeLa-G cells stably overexpressing HA-tagged RNase H1 (RNase H1) or knocked down for XPF, XPG, and CSB (shXPF, shXPG, and shCSB), respectively. "*NS" denotes a nonspecific band. (*B*) Tax induces robust GFP signal in HeLa-G and its derivatives. Following Ad-Tax transduction, cells were sparsely plated and monitored microscopically over time. Tax-expressing HeLa-G/RNase H1 (second column) and HeLa-G/shXPF, HeLa-G/shXPG, and HeLa-G/shCSB (right three columns) cells continued to divide for several cycles, while the control HeLa-G cells become irreversibly arrested in senescence as single or double GFP+ cells (left column). Details on the assay can be found in refs. 10, 12, 23, and 52. (*C*) The proliferation index of each cell line was measured as the ratio of the number of GFP+ cells on day 6 vs. day 1 after Ad-Tax transduction and was 1.42 ± 0.30 (control), 4.25 ± 1.7 (RNase H1), 15.5 ± 3.86 (shXPF), 6.34 ± 0.19 (shXPG), and 3.37 ± 0.49 (shCSB), respectively. (*D*) Immunoblots of p-KAP1, KAP1, γH2AX, and H2AX in HeLa-G and the XPF/XPG-knockdown cell lines at 12, 24, and 48 h after Ad-Tax transduction using β-actin as a loading control.

from the left). A proliferation index, defined as the ratio of the number of GFP+ cells on day 6 and that on day 1 post *tax* transduction, was used to quantify senescence resistance and was determined to be 1.42 ± 0.30 and 4.25 ± 1.7 for *tax*-transduced HeLa-G and HeLa-G/RNase H, respectively (Fig. 2*C*). As the doubling time of HeLa-G cells is ∼16 h, these data show that overexpression of RNase H1 attenuated, but did not abrogate DSB or senescence induction driven by hyperactivated NF-κB.

Down-Regulation of TC-NER Factors XPF, XPG, and CSB Mitigates Tax/NF-κB–Induced Senescence. R-loop processing is critical for repairing UV-induced DNA damage. During transcription, RNA polymerase II (RNAPII) stalls when encountering a DNA lesion such as a cyclobutene thymine dimer. Upon stalling, the RNAPII-bound nascent mRNA remains base-paired with the template DNA, displacing the nontemplate DNA strand. The DNA lesion, the RNA–DNA hybrid, and the R-loop are then detected and

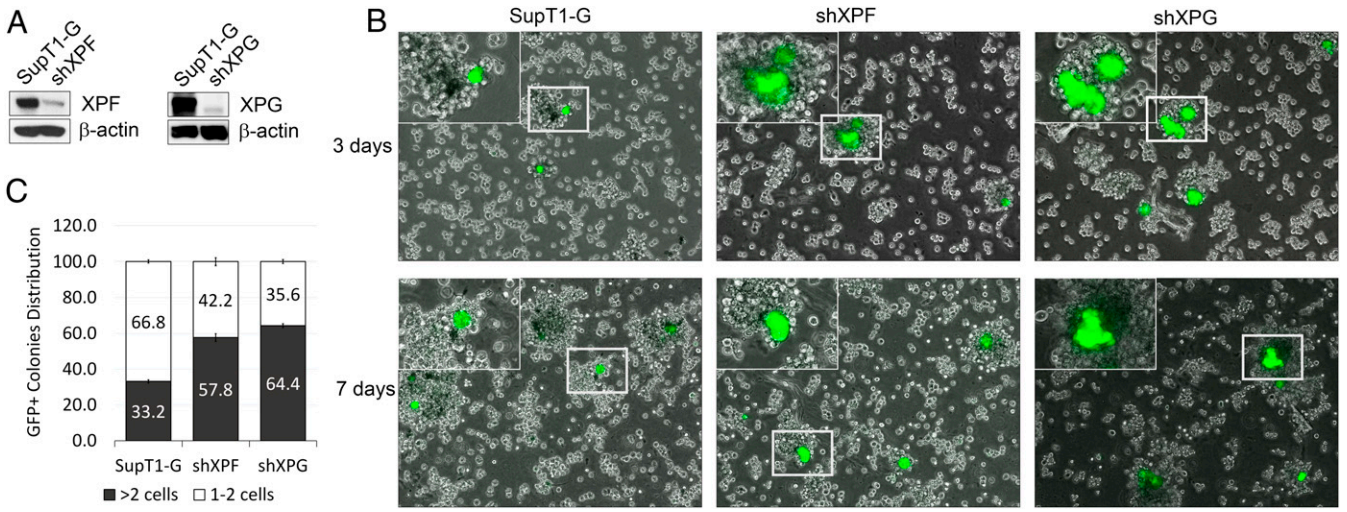

Fig. 3. XPF/XPG deficiency facilitates proliferation of HTLV-1–infected SupT1 T cells. (*A*) Immunoblots of XPF and XPG in parental SupT1-G and SupT1-G–derived cell lines stably silenced for XPF and XPG, respectively (denoted as shXPF and shXPG). (*B*) Merged fluorescence and bright-field images of HTLV-1–infected (GFP+) SupT1-G, SupT1-G/shXPF (shXPF), and SupT1-G/shXPG (shXPG) cells at 3 and 7 d post HTLV-1 infection. *Inset* in the left corner of each panel represents enlargement of the region outlined in the small rectangle. (*C*) The percentage distribution of GFP+ cell clusters consisting of one to two cells (open bars) or more than two cells (solid bars) in SupT1-G, SupT1-G/shXPF, and SupT1-G/shXPG infected by HTLV-1 on day 7 post infection ($n = 3$). Fifty GFP+ cells or cell clusters were counted for each cell line.

processed by the TC-NER pathway, which excises the lesion-containing the RNA–DNA hybrid to produce a single-strand DNA gap that is then repaired by gap-filling DNA synthesis. During TC-NER, CSB functions as a RNAPII cofactor that processes the stalled RNAPII complex, and *Xeroderma pigmentosum* F (XPF) and XPG introduce 5′ and 3′ nicks in the RNA-bound DNA strand for nucleotide excision. Importantly, Sollier et al. have previously demonstrated a crucial role of TC-NER mediators, especially XPF, XPG, and CSB, in inducing R-loop–associated DSBs and genome instability (18, 32).

To determine whether R-loop processing by TC-NER plays a role in Tax-induced DSBs and senescence, we silenced XPF, XPG, and CSB expression in HeLa-G by lentivirus vector-encoded shRNAs. Progeny HeLa-G clones were isolated (Fig. 2*A*), and the effects of the knockdowns on Tax-IRS were examined. In agreement with the R-loop model, silencing of XPF, XPG, and CSB (Fig. 2*B*, shXPF, shXPG, and shCSB columns) dampened Tax-IRS and allowed *tax*-transduced (GFP+) cells to undergo several rounds of cell division with proliferation indices of 15.5 ± 3.86, 6.34 ± 0.19, and 3.37 ± 0.49, respectively (Fig. 2*C*). Altogether, these results support the notion that R-loop–induced and TC-NER–mediated DSBs play an important role in Tax senescence. Notably, RNase H overexpression and XPF/XPG/CSB silencing attenuated, but did not prevent, Tax-IRS. Tax-induced DDR signaling persisted as indicated by the increasing levels of γH2AX and p-KAP (Fig. 2*D*) that correlated with the proliferation indices of the cell lines, suggesting that DNA replication likely also played a critical role in DNA damage induction.

XPF and XPG Silencing Enable Clonal Expansion of *tax*-Transduced or HTLV-1–Infected SupT1 and HeLa Cells. We next asked if TC-NER deficiencies could facilitate proliferative expansion of HTLV-1–infected cells. To this end, XPF and XPG expression were silenced in SupT1-G, a human CD4+ T cell line stably transduced with the 18 × 21-EGFP reporter. XPF/XPG-deficient SupT1-G cells (Fig. 3*A*) were isolated and infected with HTLV-1 after coculture with mitomycin C-treated HTLV-1–producing MT-2 cells (Fig. 3*B*) or transduced with Ad-Tax or lentiviral vector for Tax (LV-Tax) (*SI Appendix*, Fig. S1). After HTLV-1 infection or *tax* transduction, SupT1-G cells were embedded and immobilized in semisolid methylcellulose media and grown for 7 d. Consistent with the results in Fig. 2, the parental SupT1-G mostly ceased proliferation and appeared as single or double GFP+ cells after HTLV-1 infection or *tax* transduction. In contrast, similarly treated SupT1-G/shXPF or SupT1-G/shXPG expanded clonally to produce sizable multicellular GFP^+ cell clusters (Fig. 3*B* and *SI Appendix*, Fig. S1). It should be noted that HTLV-1 infection in SupT1-G occurred for only a single round, and infected cells could not spread the virus further (Fig. 3 *B*, *Left*) likely due to a lack of host factors needed for cell-to-cell virus transmission. Thus, the formation of GFP+ cell clusters results from cell proliferation. As expected, HeLa-G silenced for XPG or XPF clonally expanded after HTLV-1 infection (*SI Appendix*, Fig. S2). These results indicate that XPF and XPG deficiencies enable limited outgrowth of HTLV-1–infected T cells with Tax-mediated constitutive NF-κB activation ($NF\text{-}\kappa B^{CA}$).

ATL Cells Are Deficient in TC-NER Factors. $NF\text{-}\kappa B^{CA}$ confers survival and proliferative advantages to cancer cells (5–9, 13). We have shown previously that ATL cells, in which NF-κB is constitutively activated, have acquired genetic/epigenetic alterations that effectively prevent Tax senescence (13). As a loss of XPF, XPG, or CSB can dampen Tax-IRS, we examined HTLV-1–transformed (n = 2, C8166 and MT-4) and ATL T cell lines (n = 7, MT-1, ATL-2, ATL-T, TL-Om1, ED, ATL-35T, and ATL-55T) for evidence of XPF, XPG, and CSB down-regulation. Immunoblotting easily detected XPF, XPG, and CSB in the HTLV-1–negative Jurkat cells (Fig. 4*A*). In contrast, XPG was barely detectable in MT-1 and TL-Om1 cells (Fig. 4*A*); and likewise, XPF was expressed at low or very low levels in TL-Om1 and ED (Fig. 4*A* and see *SI Appendix*, Fig. S3 for quantitation). Finally, CSB expression was substantially down-regulated in ED (Fig. 4*A*). Overall, three of seven ATL cell lines: MT-1, TL-Om1, and ED showed significant deficit in one or more TC-NER–coupling factors compared to the HTLV-1–negative Jurkat control and other HTLV-1–transformed and ATL cell lines.

Prompted by these results, we analyzed the mRNA microarray data deposited in the National Center for Biotechnology Information (NCBI) Gene Expression Omnibus (GEO) (accession no. GSE33615) of 52 Japanese ATL patients (Fig. 4*B*, ATL) and 21 healthy donors (Fig. 4*B*, Normal) for XPF, XPG, CSB, and GAPDH expression. In agreement with the immunoblots, significant deficits in XPG, XPF, and CSB (P value <0.0001), but not in GAPDH (Fig. 4*B*, P value = 0.0610) expression were detected in the peripheral blood mononuclear cells (PBMCs) of ATL patients (Fig. 4*B*). Importantly, down-regulation of XPF, XPG, and CSB was seen across smoldering, chronic, and acute/lymphoma ATL types (Fig. 4*C*), suggesting that they occur early during ATL development. An unbiased analysis of the microarray dataset using the Qiagen Ingenuity Pathway Analysis tool also revealed NER deficiency in ATL to rank the highest in significance (– log [P value] > 50) among the alterations of DNA repair molecules (*SI Appendix*, Fig. S4), with XPG, XPB, and XPC deficiencies prominently featured (*SI Appendix*, Fig. S4*B*, genes down-regulated denoted in green), and further confirmed by immunoblotting (Fig. 4*A* and *SI Appendix*, Fig. S4*C*) and statistical analyses (*SI Appendix*, Fig. S4*D*). Overall, these data reveal in many ATL cells a significant deficit in TC-NER factors including XPF, XPG, and CSB, which likely enables adaptation to Tax-mediated $NF\text{-}\kappa B^{CA}$ during infection.

ATL Cells Are Hypersensitive to UV and Accumulate R-Loops in Abundance. Because TC-NER directs the repair of UV-induced DNA damage, we examined whether XPG/XPF-deficient MT-1, ED, and TL-Om1 might be hypersensitive to UV irradiation. Jurkat and all three ATL cell lines were subjected to UV-C at 0, 10, 20, and 40 Joules/m^2 using a UV cross-linker (XL-1000, Spectronics) The irradiated cells were grown for 5 d, and cell viability was measured by the MTS cell proliferation assay. As shown in Fig. 5*A*, compared to the Jurkat control, all three ATL lines showed hypersensitivity to UV-induced cytotoxicity, consistent with their TC-NER deficiencies. Finally, we extended the UV sensitivity study to two chronic ATL (C0013 and C0008) and two acute ATL (A0016 and A0001) patient samples. As expected, compared to the $CD4^+$ T cells of a healthy donor (phytohemagglutinin (PHA) and IL-2 stimulated and unstimulated), all $CD4^+$ T cells from ATL samples showed significantly greater sensitivity to UV irradiation, especially at lower UV-C doses (Fig. 5*B*). Statistical analyses (*SI Appendix*, Table S1) indicated that $CD4^+$ cells from all ATL patients were significantly more UV-sensitive across all UV-C doses when compared to stimulated $CD4^+$ cells from the healthy donor. The same was observed when ATL $CD4^+$ cells and unstimulated $CD4^+$ cells of the healthy donor were compared at lower UV-C doses of 10 and 20 Joules/m^2. At higher UV-C doses of 30 Joules/m^2, however, the UV-sensitivity differences between ATL and unstimulated healthy controls became obscure (Fig. 5*B*). Apparently, the greater UV sensitivity of primary $CD4^+$ T cells shifted the window of differentiation to the lower UV range. The presence of normal and latently HTLV-1–infected $CD4^+$ T cells in the ATL $CD4^+$ T cells used likely also masked the UV sensitivity of primary ATL cells in the preparation (Fig. 5*B* vs. Fig. 5*A*).

We have previously reported that NF-κB is constitutively active in MT-1, ED, and TL-Om1 (13). As confirmed in Fig. 5*C*, all three cell lines showed increased RelB levels, NF-κB2 p100 processing

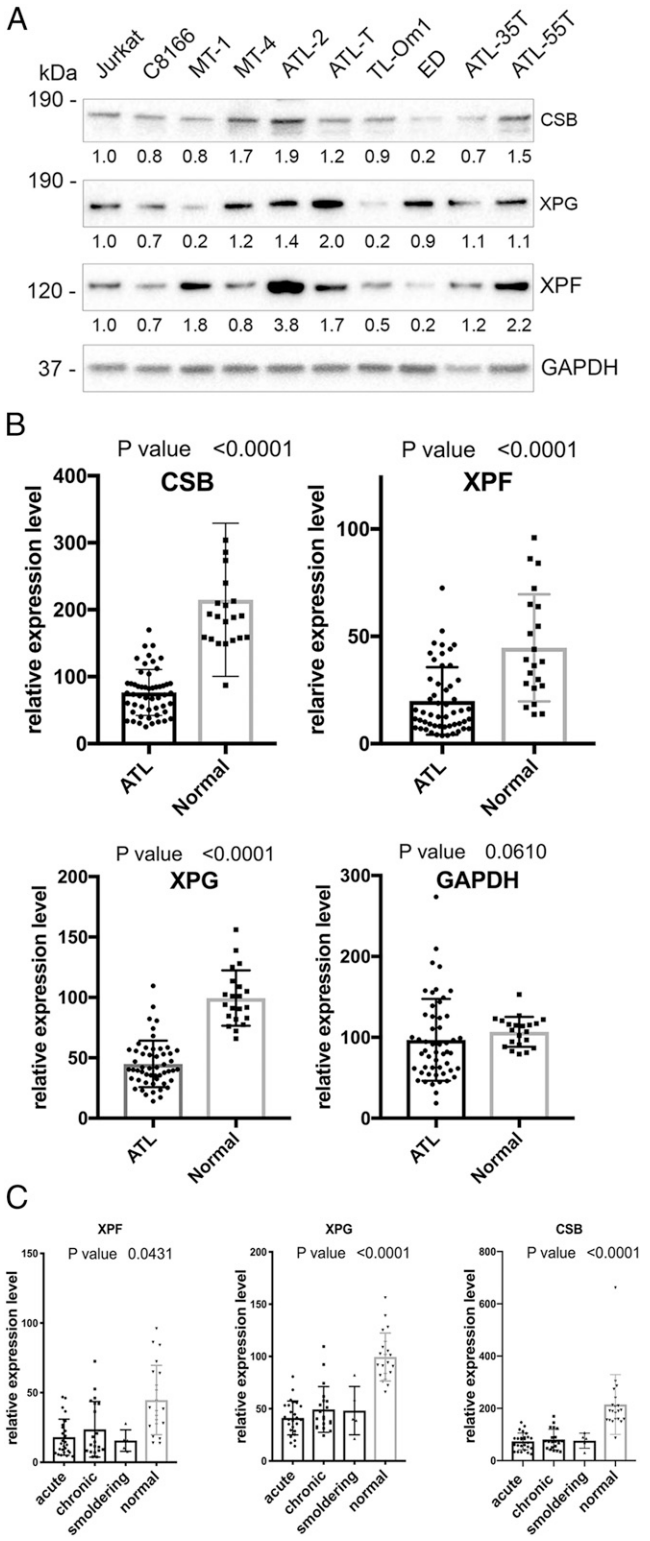

Fig. 4. ATL cells are deficient in XPF, XPG, and CSB. (*A*) Immunoblots of ATL (MT-1, ATL-T, ATL-2, TL-Om1, ED, ATL-35T, and ATL-55T) and HTLV-1–transformed T cell lines (C8166 and MT4) vs. HTLV-1–negative T cell lines (SupT1, Jurkat, and CEM). The proteins immunoblotted and their molecular sizes are indicated on the right and left, respectively. The relative levels of expression were normalized first to GAPDH and then to Jurkat control (*SI Appendix*, Fig. S3). The immunoblots were repeated three times with one representative blot shown. The number under each lane indicates the relative level of expression. (*B*) The relative mRNA expression of 52 ATL patients and 21 healthy donors (normal) were based on the ATL microarray dataset GSE33615 deposited in the NCBI GEO repository. The expression level of each gene was normalized to the cognate β-actin. Mann–Whitney *U* test was performed to compare the normalized expression levels of ATL patients (ATL) and healthy donors (Normal) using the GraphPad PRISM (8.0c) software. (*C*) Relative XPF, XPG, and CSB mRNA expression in acute, chronic, and smoldering ATL patients and normal blood donors. Relative XPF, XPG, and CSB mRNA expression levels in the PBMCs of smoldering ($n = 5$), chronic ($n = 20$), or acute ATL ($n = 27$) patients vs. those in CD4+ T lymphocytes of healthy blood donors ($n = 21$). The microarray dataset contains one lymphoma case and one unknown/unclassified case that were grouped with the acute and the smoldering cases. respectively.

to p52, and elevated levels of phospho-IκBα. Because IκBα and phospho-IκBα levels in ED were low, we treated ED and the Jurkat control with the proteasome inhibitor MG132 in a time course. As expected, a markedly higher level of phospho-IκBα accumulated in ED upon MG132 treatment compared to the Jurkat control (Fig. 5*D*), consistent with constitutive NF-κB activation.

To demonstrate that constitutive NF-κB activation causes ATL cells to accumulate excess R-loops, we extracted chromosomal nucleic acids from MT-1, TL-Om1, ED, and Jurkat and SupT1 controls and probed them with the S9.6 antibody. As shown in Fig. 5*E*, R-loop signals in MT-1, TL-Om1, and ED were significantly higher than those of the SupT1 and Jurkat controls. As expected, the R-loop signals disappeared upon sample treatment with RNase H (Fig. 5*F*). In aggregate, these results demonstrate that TC-NER deficiencies facilitate adaptation to constitutively activated NF-κB and aid the proliferative expansion of HTLV-1–infected and ATL cells, but render them hypersensitive to UV irradiation. The accumulation of excess R-loops in ATL also raises the possibility that a restoration of the expression of TC-NER factors may increase R-loop–induced DSBs, thereby drive ATL cells to senescence or apoptosis.

Discussion

Approximately 3 to 5% of HTLV-1–infected individuals develop ATL decades after infection (33, 34). Two viral regulatory proteins, Tax and HBZ, are thought to play crucial roles in ATL development (35, 36). Tax is a potent activator of IKK/NF-κB (1), and yet NF-κB activation by Tax leads immediately to cellular senescence (23). Here we have demonstrated that Tax-mediated NF-κB hyperactivation promotes R-loop accumulation and that R-loop processing by TC-NER contributes to the induction of DSBs and senescence. Our results indicate that RNase H1 overexpression and shRNA silencing of the TC-NER–coupling factors XPF, XPG, and CSB attenuate Tax senescence and enable outgrowth and expansion of *tax*-transduced or HTLV-1–infected cells, a precursor event to ATL development (37). Importantly, we have found that many ATL cells are TC-NER–deficient and hypersensitive to UV-induced cytotoxicity. We have recently demonstrated that ATL cells downregulate the expression of a key DDR mediator, RING finger protein 8 (RNF8), which is critical for signaling repair of DSBs (38) and Tax-mediated canonical NF-κB activation (39). As UV irradiation also leads to DSBs, RNF8 deficiency likely exacerbates the cytotoxicity of UV for TC-NER–deficient ATL cells. These data correlate with a recent clinical study showing that smoldering ATL patients treated with UV-based phototherapy achieved a complete response with a significantly extended time of survival (40). We noted that primary $CD4^+$ cells, regardless of whether they originated from ATL patients or healthy donors, were more sensitive to UV in general (compare Fig. 5 *A* and *B*). This shifted the UV sensitivity window that differentiated between ATL and normal CD4+ T cells to lower UV-C doses up to 20 Joules/m^2 (Fig. 5*B* and *SI Appendix*, Table S1). The ATL $CD4^+$ T cells used here contained, in addition to ATL cells,

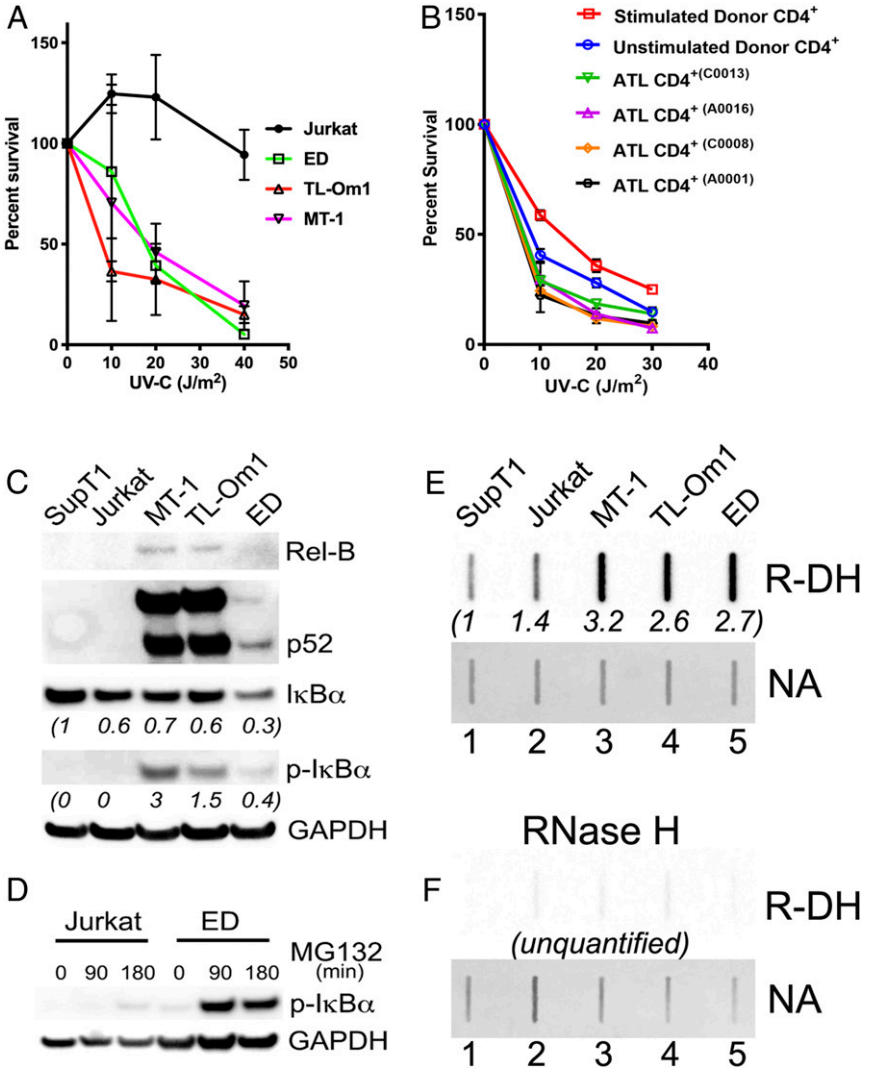

Fig. 5. ATL cells are hypersensitive to UV and accumulate R-loops in abundance. (*A*) UV sensitivity of ATL (ED, TL-Om1, and MT-1) cell lines and Jurkat control. The UV-C dose used in each treatment is as indicated. Cell viability was determined by the MTS assay (*Materials and Methods*). Three replicates were performed for each data point. A representative figure is shown. (*B*) UV sensitivity of $CD4^+$ T Cells from a healthy donor (stimulated and unstimulated with IL-2) and four ATL patients (two chronic and two acute ATL cases). The UV-C doses used in each treatment are as indicated. Cell viability was determined by the Alamar Blue cell proliferation assay. The statistical significance of the comparison between the UV sensitivities of ATL and normal CD4+ cells is tabulated in *SI Appendix*, Table S1. (*C* and *D*) Constitutive NF-κB Activation in ATL cells. (*C*) Whole-cell lysates of ATL (MT, TL-Om1, ED) and control (SupT1 and Jurkat) CD+ T cell lines were analyzed for the expression of the indicated proteins by immunoblotting. (*D*) ED and Jurkat were treated with the proteasome inhibitor MG132 for the indicated times and immunoblotted. (*E* and *F*) ATL cells accumulate excess R-loops. (*E*) Chromosomal nucleic acids were extracted from SupT1, Jurkat, ED, TL-Om1, and MT-1 cells and slot-blotted as in Fig. 1 using the S9.6 antibody and quantified in the same manner as in Fig. 1*B*. (*F*) RNase H treatment and R-loop (R-DH) and nucleic acids (NA) detection were similarly performed as above.

latent HTLV-1–infected and normal $CD4^+$ T cells. The UV sensitivity seen with ATL $CD4^+$ T cells (Fig. 5*B*) was likely masked by the presence of nonleukemic $CD4^+$ T cells and was not as dramatic as when ATL cell lines were used (Fig. 5*A*). Further purification of ATL cells was technically challenging, especially when only small amounts of clinical samples were available. Finally, TC-NER–deficient ATL cells with constitutively activated NF-κB continue to accumulate R-loops, raising the possibility that, upon restoration of TC-NER function, these cells may develop extensive DSBs and undergo cell-cycle arrest/senescence/apoptosis. Thus, our results, summarized schematically in Fig. 6, have revealed specific vulnerabilities in ATL that can be therapeutically targeted.

Leukemia cells in many (>50%) ATL patients no longer express Tax (41, 42) and have evolved gain-of-function mutations that drive Tax-independent $NF\text{-}\kappa B^{CA}$ (35). We think this is facilitated by the TC-NER deficiencies positively selected for during persistent infection and maintained in ATL (Fig. 6). As many T/B cell malignancies, including peripheral and cutaneous T cell lymphoma (43), diffuse large B cell lymphoma (44), chronic lymphocytic leukemia (CLL) (8), and multiple myeloma (MM) (9), rely on $NF\text{-}\kappa B^{CA}$ for proliferation and survival, they likely also harbor TC-NER deficiencies. Several recent publications describing the successful targeting of TC-NER in CLL (45) and NER in MM (46) support this conclusion.

The $Tax/NF\text{-}\kappa B^{CA}$-driven DSBs and RNF8 and TC-NER deficiencies promote genomic instability in HTLV-1–infected and ATL cells. The R-loop model predicts that DSBs are prone to occur within Tax/NF-κB–induced genes. A recent whole-genome sequencing analysis (35) has revealed many ATL-significant genes that are altered by insertions and deletions (indels), including A20/TNFAIP3, B2M, FAS, GATA3, HLA-B, and TP53, are

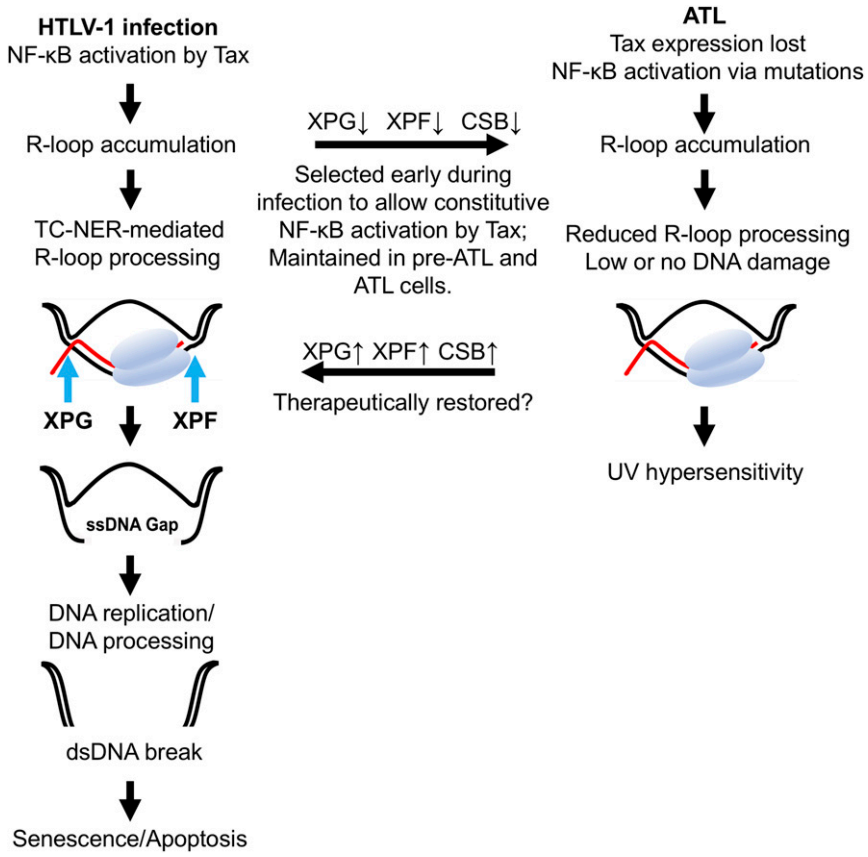

Fig. 6. HTLV-1 infection and NF-κB–induced R-loop accumulation select for transcription-coupled nucleotide excision repair deficits in adult T cell leukemia. DNA double helix and mRNA are depicted in black and red, respectively. (*Left*) NF-κB hyperactivation by Tax during HTLV-1 infection leads to R-loop accumulation. During R-loop processing, XPF and XPG cleaves at the 5′ and 3′ ends of the RNA-bound DNA strand in R-loop to generate a single-stranded DNA (ssDNA) gap. DNA replication and/or additional ssDNA processing leads to DNA double-strand breaks and senescence. (*Middle Top*) T cells deficient in TC-NER undergo clonal expansion after HTLV-1 infection and evolve into ATL cells that are hypersensitive to UV irradiation. (*Right*) Somatic mutations develop in ATL to drive Tax-independent NF-κB activation. NF-κB–induced R-loops continue to accumulate, but do not induce DSBs due to down-regulation of TC-NER mediators and other alterations. (*Middle Bottom*) Restoration of TC-NER function in these ATL cells is expected to increase R-loop processing, leading to DSBs and senescence/cell death.

Tax/NF-κB targets. Experiments are currently underway to assess the involvement of R-loop–associated DSBs in causing these indels. It is interesting to note that several of these genes encode negative regulators of the IKK/NF-κB signal transduction pathway, molecules involved in immune surveillance, or tumor suppressors.

RNase H overexpression and XPF/XPG/CSB silencing attenuated but did not prevent Tax-IRS. Tax-induced DDR signaling persisted in cells depleted of XPF or XPG (Fig. 2*D*), suggesting that R-loop processing by TC-NER cannot fully account for the DSBs that lead to senescence. Other genome destabilizing activities of Tax, including aberrant activation of RNF8 and mislocalization of DDR factors, likely also play a role (2, 47, 48). Interestingly, Tax-induced DSBs and DDR signaling correlated with the proliferation indices of the knockdown cell lines (Fig. 2 *C* and *D*), suggestive of the involvement of DNA replication in transcription-/R-loop–associated DSBs (15, 16, 18). In this vein, our published data have indicated that, upon cell entry into the S phase, Tax-induced p21 expression increases dramatically (10, 31) and Tax-IRS requires cell-cycle passage through S/G2/M (10). It has been proposed recently that head-on transcription-replication conflicts promote R-loop accumulation and exacerbate DNA damage and genomic instability (49, 50). Elucidating how DNA replication impacts Tax/NF-κB^{CA}–induced and transcription-mediated DNA damage and senescence may reveal additional vulnerabilities in ATL that can be targeted clinically.

Materials and Methods

Cell Lines and Cell Culture. Human T cell lines were cultured in Roswell Park Memorial Institute (RPMI) 1640 (HyClone) supplemented with 10% fetal bovine serum (FBS), L-glutamine, and 100 U/mL penicillin and streptomycin and maintained in 5% CO_2 at 37 °C. HeLa-G and its progeny cell lines were grown in Dulbecco's Modified Eagle Media (Quality Biologicals) containing 10% FBS. PBMCs from de-identified healthy donors and chronic and acute ATL patients were cultured in RPMI 1640 media (Gibco, catalog #22400089) supplemented with 10% FBS, 100 U/mL penicillin and streptomycin, and 50 μM 2-mercaptoethanol for 1 d. PBMCs from healthy donors were either stimulated or unstimulated with IL-2 and 1.5% phytohemagglutinin (Gibco, catalog #10576015) for 2 d. $CD4^+$ T cells from the PBMCs of healthy donors and ATL patients were enriched using a human $CD4^+$ T cell isolation kit (Miltenyi Biotec, catalog #130–091-301) following the manufacturer's protocol. To ensure the purity of CD4+ cells, PBMCs were treated with the same kit twice to remove non-$CD4^+$ cells. Greater than 95% of the purified cells were $CD4^+$, and, of the $CD4^+$ population, more than 70% were $CD25^+$, which represents the ATL cells.

Lentiviral Vectors. Derivation of the LV-Tax and SMPU-18 × 21-EGFP has been described previously (23, 30). The vector for the HA-tagged human RNase H1, LV-RNase H1, was similarly derived.

R-Loop Detection. Genomic DNAs of HeLa-G cells transduced with Ad-Tax or Ad-GFP (multiplicity of infection [moi]: ~5) were isolated using the SDS-proteinase K extraction method (51) and slot-blotted (1 μg) with the S9.6 antibody (28) to detect RNA–DNA hybrids as a marker of R-loops. The equal

amount of nucleic acid loaded in each slot was confirmed by methylene blue (final concentration 0.025%) staining.

Knockdown of XPF, XPG, and CSB Genes. HeLa-G and SupT1-G cell lines with stable knockdown of each of the three genes were isolated by screening cell clones among cells transduced by pooled shRNA lentiviral vectors. All shRNA lentiviral vectors harbor the puromycin-resistance gene. The sequences targeted in each gene are as listed (*SI Appendix*, Table S2).

Growing HTLV-1–Infected or *tax*-Transduced T Cells in Semisolid Medium. Methyl cellulose solution (4% wt/vol, Sigma M-0512) was autoclaved and cooled to 4 °C. The solution was mixed with equal volume of 2 x RPMI medium (HyClone) (2 x RPMI + 20% FBS + penicillin/streptomycin + glutathione) to make a 2% semisolid stock medium, which was kept in solution at 4 °C. SupT1-G T cells transduced with LV-Tax or infected by HTLV-1 were harvested, resuspended in RPMI medium, mixed with equal volume of 2% semisolid stock medium, and plated dropwise into a six-well plate. The embedded cells were grown at 37 °C in a CO_2 incubator. GFP^+ T cells were monitored for 7 to 10 d.

HTLV-1 Infection in Cell Culture. HTLV-1–producing MT-2 cells were treated with 10 μg/mL mitomycin C (Selleckchem, S8146) for 2 h and then washed twice with RPMI medium and mixed with SupT1-G or progeny cell lines at 5:1 ratio and incubated in a well of a 24-well plate for 24 h. Thereupon, cells were embedded in 1% semisolid medium containing 1 mM Raltegravir (Selleckchem, S2005) to prevent further infection. The infected GFP+ cells were incubated for 7 d, and cell proliferation was monitored visually by fluorescence microscopy.

UV Sensitivity Determination. A total of 40,000 T cells were grown in 1.5 mL of RPMI containing 10% FBS per well in a six-well plate. The cell suspension was subjected to UV-C irradiation at the indicated doses and returned to the CO_2 incubator. After 120 h of incubation, the cell suspension was transferred to a 96-well plate in aliquots of 100 μL per well, and cell viability was measured using a MTS proliferation assay. Percentage survival was calculated by normalizing the absorbance readings of irradiated cells with those of untreated cells. Percentage survivability of untreated cells was set at 100%. Three absorbance readings were carried out for each condition, and the mean percentage survival was calculated. Two to three independent replicates were carried out with Jurkat as a control. The UV sensitivity of primary $CD4^+$ T cells was similarly determined. A total of 200,000 $CD4^+$ T cells from each healthy donor (either stimulated or unstimulated with PHA and IL-2) and from chronic and acute ATL patients were grown in 500 μL RPMI-1640 medium supplemented with 10% FBS per well in a 24-well plate. The cells were subject to UV-C irradiation at the indicated doses using a Spectrolinker XL-1000 UV cross-linker and returned to the CO_2 incubator. After 24 h of incubation, ~20,000 cells of each sample were transferred to a 96-well plate in aliquots of 90 μL per well, and cell viability was measured using the Alamar blue cell proliferation reagent (Invitrogen, catalog #A50100). Percentage survival was calculated as described above.

Immunoblotting. Standard methods were used for immunoblotting. Cells were harvested and lysed in lysis buffer (Cell Signaling). Samples typically contain 25 μg of whole-cell proteins as determined by BCA assay (Promega). The HTLV-1 Tax mouse hybridoma monoclonal antibody 4C5 was generated in our laboratory as previously described (31). All other antibodies were commercially available and as listed in *SI Appendix*, Table S3.

Quantitation and Statistical Analysis. The accession number for the whole-genome gene expression profiles of ATL is GSE33615. PRISM 8.0 and Image J were used for statistical analysis of gene expression and quantitation of immunoblots. The expression value of a given gene in each individual was normalized against that of the cognate β-actin. The relative expression values of ATL patients (n = 52, PBMCs) and healthy blood donors (n = 21, CD4+ T cells) were compared using the Mann–Whitney U test. The microarray dataset contains one lymphoma case and one unknown/unclassified case that were grouped with the acute and the smoldering cases, respectively. The proliferation index used to quantify the degree of senescence or senescence resistance post *tax* transduction is defined as the ratio of the number of GFP+ cells on day 6 and on day 1. For control naive cells that become senescent after HTLV-1 infection of *tax* transduction, the proliferation index is ~1.4.

Data Availability. All study data are included in the article and/or *SI Appendix*.

ACKNOWLEDGMENTS. We thank Masao Matsuoka for the ATL cell lines, Cara Olsen for advice on statistical analysis, David Horowitz for the UV irradiator, and Brian Schaefer for critical reading of the manuscript. This work was supported by grants from the NIH (R21CA216660) and Uniformed Services University (HU0001-14-1-0061). The opinions and assertions expressed herein are those of the author's and do not necessarily reflect the official policy or position of the Uniformed Services University or the Department of Defense.

1. E. W. Harhaj, C. Z. Giam, NF-κB signaling mechanisms in HTLV-1-induced adult T-cell leukemia/lymphoma. *FEBS J.* **285**, 3324–3336 (2018).
2. Y. K. Ho *et al.*, HTLV-1 tax stimulates ubiquitin E3 ligase, ring finger protein 8, to assemble lysine 63-linked polyubiquitin chains for TAK1 and IKK activation. *PLoS Pathog.* **11**, e1005102 (2015).
3. D. A. Rauch, L. Ratner, Targeting HTLV-1 activation of NFκB in mouse models and ATLL patients. *Viruses* **3**, 886–900 (2011).
4. Y. Shibata *et al.*, HTLV-1 tax induces formation of the active macromolecular IKK complex by generating Lys63- and Met1-linked hybrid polyubiquitin chains. *PLoS Pathog.* **13**, e1006162 (2017).
5. R. D. Morin *et al.*, Mutational and structural analysis of diffuse large B-cell lymphoma using whole-genome sequencing. *Blood* **122**, 1256–1265 (2013).
6. L. Pasqualucci *et al.*, Analysis of the coding genome of diffuse large B-cell lymphoma. *Nat. Genet.* **43**, 830–837 (2011).
7. V. N. Ngo *et al.*, Oncogenically active MYD88 mutations in human lymphoma. *Nature* **470**, 115–119 (2011).
8. G. Fabbri, R. Dalla-Favera, The molecular pathogenesis of chronic lymphocytic leukaemia. *Nat. Rev. Cancer* **16**, 145–162 (2016).
9. M. A. Chapman *et al.*, Initial genome sequencing and analysis of multiple myeloma. *Nature* **471**, 467–472 (2011).
10. L. Yang *et al.*, Complex cell cycle abnormalities caused by human T-lymphotropic virus type 1 Tax. *J. Virol.* **85**, 3001–3009 (2011).
11. M. Liu *et al.*, Human T-cell leukemia virus type 1 infection leads to arrest in the G1 phase of the cell cycle. *J. Virol.* **82**, 8442–8455 (2008).
12. S. Philip, M. A. Zahoor, H. Zhi, Y. K. Ho, C. Z. Giam, Regulation of human T-lymphotropic virus type I latency and reactivation by HBZ and Rex. *PLoS Pathog.* **10**, e1004040 (2014).
13. A. M. D. Shudofsky, C. Z. Giam, Cells of adult T-cell leukemia evade HTLV-1 Tax/NF-κB hyperactivation-induced senescence. *Blood Adv.* **3**, 564–569 (2019).
14. Y. K. Ho *et al.*, HTLV-1 tax-induced rapid senescence is driven by the transcriptional activity of NF-κB and depends on chronically activated IKKα and p65/RelA. *J. Virol.* **86**, 9474–9483 (2012).
15. J. Sollier, K. A. Cimprich, Breaking bad: R-Loops and genome integrity. *Trends Cell Biol.* **25**, 514–522 (2015).
16. J. M. Santos-Pereira, A. Aguilera, R loops: New modulators of genome dynamics and function. *Nat. Rev. Genet.* **16**, 583–597 (2015).
17. L. Wahba, J. D. Amon, D. Koshland, M. Vuica-Ross, RNase H and multiple RNA biogenesis factors cooperate to prevent RNA:DNA hybrids from generating genome instability. *Mol. Cell* **44**, 978–988 (2011).
18. J. Sollier *et al.*, Transcription-coupled nucleotide excision repair factors promote R-loop-induced genome instability. *Mol. Cell* **56**, 777–785 (2014).
19. F. d'Adda di Fagagna *et al.*, A DNA damage checkpoint response in telomere-initiated senescence. *Nature* **426**, 194–198 (2003).
20. J. Bartkova *et al.*, Oncogene-induced senescence is part of the tumorigenesis barrier imposed by DNA damage checkpoints. *Nature* **444**, 633–637 (2006).
21. J. Campisi, Cellular senescence as a tumor-suppressor mechanism. *Trends Cell Biol.* **11**, S27–S31 (2001).
22. J. P. Coppé, P. Y. Desprez, A. Krtolica, J. Campisi, The senescence-associated secretory phenotype: The dark side of tumor suppression. *Annu. Rev. Pathol.* **5**, 99–118 (2010).
23. H. Zhi *et al.*, NF-κB hyper-activation by HTLV-1 tax induces cellular senescence, but can be alleviated by the viral anti-sense protein HBZ. *PLoS Pathog.* **7**, e1002025 (2011).
24. F. Majone, O. J. Semmes, K. T. Jeang, Induction of micronuclei by HTLV-I tax: A cellular assay for function. *Virology* **193**, 456–459 (1993).
25. O. J. Semmes *et al.*, HTLV-I and HTLV-II tax: Differences in induction of micronuclei in cells and transcriptional activation of viral LTRs. *Virology* **217**, 373–379 (1996).
26. H. H. Baydoun, X. T. Bai, S. Shelton, C. Nicot, HTLV-I tax increases genetic instability by inducing DNA double strand breaks during DNA replication and switching repair to NHEJ. *PLoS One* **7**, e42226 (2012).
27. J. D. Amon, D. Koshland, RNase H enables efficient repair of R-loop induced DNA damage. *eLife* **5**, e20533 (2016).
28. C. T. Stork *et al.*, Co-transcriptional R-loops are the main cause of estrogen-induced DNA damage. *eLife* **5**, e17548 (2016).
29. X. Li, J. L. Manley, Inactivation of the SR protein splicing factor ASF/SF2 results in genomic instability. *Cell* **122**, 365–378 (2005).
30. L. Zhang, M. Liu, R. Merling, C. Z. Giam, Versatile reporter systems show that transactivation by human T-cell leukemia virus type 1 Tax occurs independently of chromatin remodeling factor BRG1. *J. Virol.* **80**, 7459–7468 (2006).
31. Y. L. Kuo, C. Z. Giam, Activation of the anaphase promoting complex by HTLV-1 tax leads to senescence. *EMBO J.* **25**, 1741–1752 (2006).

32. Y. L. Lin, P. Pasero, Caught in the act: R-Loops are cleaved by structure-specific endonucleases to generate DSBs. *Mol. Cell* **56**, 721–722 (2014).
33. G. P. Taylor, M. Matsuoka, Natural history of adult T-cell leukemia/lymphoma and approaches to therapy. *Oncogene* **24**, 6047–6057 (2005).
34. M. Matsuoka, K. T. Jeang, Human T-cell leukaemia virus type 1 (HTLV-1) infectivity and cellular transformation. *Nat. Rev. Cancer* **7**, 270–280 (2007).
35. K. Kataoka *et al*., Integrated molecular analysis of adult T cell leukemia/lymphoma. *Nat. Genet.* **47**, 1304–1315 (2015).
36. C. Z. Giam, O. J. Semmes, HTLV-1 infection and adult T-cell leukemia/lymphoma—A tale of two proteins: Tax and HBZ. *Viruses* **8**, 161 (2016).
37. S. Firouzi *et al*., Clonality of HTLV-1-infected T cells as a risk indicator for development and progression of adult T-cell leukemia. *Blood Adv.* **1**, 1195–1205 (2017).
38. N. K. Kolas *et al*., Orchestration of the DNA-damage response by the RNF8 ubiquitin ligase. *Science* **318**, 1637–1640 (2007).
39. H. Zhi *et al*., RNF8 dysregulation and down-regulation during HTLV-1 infection promote genomic instability in adult T-cell leukemia. *PLoS Pathog.* **16**, e1008618 (2020).
40. P. D. Oliveira *et al*., Adult T-cell leukemia/lymphoma treatment in Bahia, Brazil. *Rev. Bras. Hematol. Hemoter.* **39**, 13–19 (2017).
41. S. Takeda *et al*., Genetic and epigenetic inactivation of tax gene in adult T-cell leukemia cells. *Int. J. Cancer* **109**, 559–567 (2004).
42. C. R. Bangham *et al*., The immune control of HTLV-1 infection: Selection forces and dynamics. *Front. Biosci.* **14**, 2889–2903 (2009).
43. A. J. Moskowitz, S. M. Horwitz, Targeting histone deacetylases in T-cell lymphoma. *Leuk. Lymphoma* **58**, 1306–1319 (2017).
44. A. Reddy *et al*., Genetic and functional drivers of diffuse large B cell lymphoma. *Cell* **171**, 481–494.e15 (2017).
45. G. Lohmann *et al*., Targeting transcription-coupled nucleotide excision repair overcomes resistance in chronic lymphocytic leukemia. *Leukemia* **31**, 1177–1186 (2017).
46. R. Szalat *et al*., Nucleotide excision repair is a potential therapeutic target in multiple myeloma. *Leukemia* **32**, 111–119 (2018).
47. A. Haoudi, R. C. Daniels, E. Wong, G. Kupfer, O. J. Semmes, Human T-cell leukemia virus-I tax oncoprotein functionally targets a subnuclear complex involved in cellular DNA damage-response. *J. Biol. Chem.* **278**, 37736–37744 (2003).
48. S. S. Durkin *et al*., HTLV-1 Tax oncoprotein subverts the cellular DNA damage response via binding to DNA-dependent protein kinase. *J. Biol. Chem.* **283**, 36311–36320 (2008).
49. S. Hamperl, M. J. Bocek, J. C. Saldivar, T. Swigut, K. A. Cimprich, Transcription-replication conflict orientation modulates R-loop levels and activates distinct DNA damage responses. *Cell* **170**, 774–786.e19 (2017).
50. M. P. Crossley, M. Bocek, K. A. Cimprich, R-loops as cellular regulators and genomic threats. *Mol. Cell* **73**, 398–411 (2019).
51. T. Maniatis, E. F. Fritsch, J. Sambrook, *Molecular Cloning: A Laboratory Manual* (Cold Spring Harbor Laboratory Press, Cold Spring Harbor, NY, 1982).
52. H. Zhi, M. A. Zahoor, A. M. Shudofsky, C. Z. Giam, KSHV vCyclin counters the senescence/G1 arrest response triggered by NF-kappaB hyperactivation. *Oncogene* **34**, 496–505 (2015).